

Positron Emission Tomography (PET) and Pharmacokinetics: Classical Blood Sampling Versus Image-Derived Analysis of [¹⁸F]FAZA and [¹⁸F]FDG in a Murine Tumor Bearing Model

Hans-Soenke Jans¹, Xiao-Hong Yang¹, Dion R Brocks², Piyush Kumar¹, Melinda Wuest¹, and Leonard I Wiebe^{1,2}

¹Department of Oncology, Faculty of Medicine and ²Faculty of Pharmacy and Pharmaceutical Sciences, University of Alberta, Edmonton, Canada

Received, February 6, 2018; Revised, March 4, 2018; Accepted, April 17, 2018; Published, April 20, 2018.

ABSTRACT - Purpose: Pharmacokinetic (PK) data are generally derived from blood samples withdrawn serially over a defined period after dosing. In small animals, blood sampling after dosing presents technical difficulties, particularly when short time intervals and frequent sampling are required. Positron emission tomography (PET) is a non-invasive functional imaging technique that can provide semi-quantitative temporal data for defined volume regions of interest (vROI), to support kinetic analyses in blood and other tissues. The application of preclinical small-animal PET to determine and compare PK parameters for [¹⁸F]FDG and [¹⁸F]FAZA, radiopharmaceuticals used clinically for assessing glucose metabolism and hypoxic fractions, respectively, in the same mammary EMT6 tumor-bearing mouse model, is reported here. **Methods:** Two study groups were used: normal BALB/c mice under isoflurane anesthesia were intravenously injected with either [¹⁸F]FDG or [¹⁸F]FAZA. For the first group, blood-sampling by tail artery puncture was used to collect blood samples which were then analyzed with Radio-microTLC. Dynamic PET experiments were performed with the second group of mice and analyzed for blood input function and tumor uptake utilizing a modified two compartment kinetic model. Heart and inferior vena cava vROIs were sampled to obtain image-derived data. PK parameters were calculated from blood samples and image-derived data. Time-activity curves (TACs) were also generated over regions of liver, kidney and urinary bladder to depict clearance profiles for each radiotracer. **Results:** PK values generated by classical blood sampling and PET image-derived analysis were comparable to each other for both radiotracers. Heart vROI data were suitable for analysis of [¹⁸F]FAZA kinetics, but metabolic uptake of radioactivity mandated the use of inferior vena cava vROIs for [¹⁸F]FDG analysis. While clearance (CL) and blood half-life (t_{1/2}) were similar for both [¹⁸F]FDG and [¹⁸F]FAZA for both sampling methods, volume of distribution yielded larger differences, indicative of limitations such as partial volume effects within quantitative image-derived data. [¹⁸F]FDG underwent faster blood clearance and had a shorter blood half-life than [¹⁸F]FAZA. Kinetic analysis of tumor uptake from PET image data showed higher uptake and longer tumor tissue retention of [¹⁸F]FDG, indicative of the tumor's glucose metabolism rate, versus lower tumor uptake and retention of [¹⁸F]FAZA. While [¹⁸F]FAZA possesses a somewhat greater hepatobiliary clearance, [¹⁸F]FDG clears faster through the renal system which results in faster radioactivity accumulation in the urinary bladder. **Conclusions:** The present study provides a working example of the applicability of functional PET imaging as a suitable tool to determine PK parameters in small animals. The comparative analysis in the current study demonstrates that it is feasible to use [¹⁸F]FDG PET and [¹⁸F]FAZA PET in the same model to analyze their blood PK parameters, and to estimate kinetic parameters for these tracers in tumor. This non-invasive imaging-based determination of tissue kinetic parameters facilitates translation from pre-clinical to clinical phases of drug development.

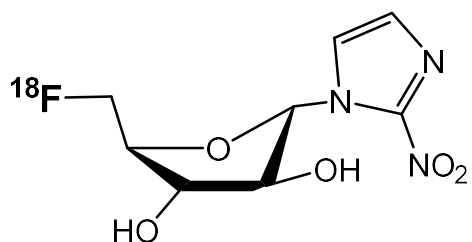
This article is open to **POST-PUBLICATION REVIEW**. Registered readers (see "For Readers") may **comment** by clicking on ABSTRACT on the issue's contents page.

INTRODUCTION

Positron emission tomography (PET) using hypoxia-selective radiotracers is a viable, effective approach for clinical imaging of tumour hypoxia [1,2]. 1-[¹⁸F]Fluoro-3-(2-nitro-imidazol-1-yl)-propan-2-ol

Corresponding Author: Leonard I Wiebe, Div. of Oncologic Imaging, Dept. of Oncology, Faculty of Medicine and Dentistry, 2-40 MICEF, South Campus, University of Alberta; E-mail: leonard.wiebe@ualberta.ca

(^{18}F)FMISO), a first generation hypoxia PET imaging agent [3] and 1- α -D-(5-deoxy-5- ^{18}F)fluoroarabinofuranosyl)-2-nitroimidazole (^{18}F)FAZA; **Fig. 1**) an established second generation PET radiotracer, were developed for that purpose [4-6]. As reported by many studies to date, both compounds selectively accumulate in tumor cells under hypoxic conditions and are widely used clinically to assess tumor hypoxia [7]. In contrast to ^{18}F FMISO, which is the more lipophilic radiotracer, ^{18}F FAZA is characterized by faster clearance from blood and non-target tissues such as muscle and overall body, to result in faster



development of image contrast in preclinical and clinical studies [5,8].

To date, 2-deoxy-2- ^{18}F fluoro-D-glucopyranose (^{18}F)FDG; **Fig. 1**) remains the most widely used clinical PET radiopharmaceutical tracer. Its development represented a major breakthrough in both fluorine chemistry [9,10] and F-18 chemistry [11,12]. ^{18}F FDG's specificity as a substrate for hexokinase and facilitative glucose transport (GLUTs) has made it the preferred diagnostic PET tracer in oncology, cardiology, neurology, and other conditions [13].

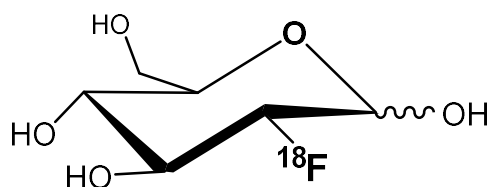


Figure 1. Chemical structures of ^{18}F FAZA (left) and ^{18}F FDG (right).

Pharmacokinetics (PK) describe the time course of drug handling in living organisms [14] and can provide insight into mechanisms of drug clearance from blood and first pass metabolism. PK provides the basis for logical understanding of the relationships between drug concentrations in blood, overall distribution within the body, and excretion, thereby enabling rationalization of therapeutic and / or toxic effects of drugs in relation to various therapeutic regimens [15].

Measuring drug movement through different membrane barriers, however, is more challenging than measuring concentrations of drug and/or metabolites in blood. Modelling the uptake and subsequent clearance of a drug from an anatomical site using conventional compartmental blood analysis is possible only if invasive measurement techniques, like biopsy, are used. Normally classical PK does not identify specific anatomical or biochemical compartments, especially if multistep processes are involved. Analysis of clinical tissue biopsies can provide the required tissue information, but their invasive nature makes them less acceptable to patients and practitioners alike. Collecting data from preclinical animal models, where biopsy and blood sampling are ethically less problematic, can be

used for *in vivo* kinetic modeling, which may then be translated into the human setting. Microsampling can help to increase the quality of the PK analysis [16], and together with improved methods of chemical analysis [17,18], and technological advances such as non-invasive functional imaging, suitable tools are now in hand to generate more realistic *in vivo* data for translational drug development of a chemical compound from bench-to bedside [19]. Consequently, non-invasive techniques such as functional PET imaging are utilized more frequently in both pre-clinical and clinical kinetic investigations.

Functional imaging technologies such as PET have added more tools for studying and understanding drug kinetics and metabolism, and PET-based kinetic pre-clinical studies contribute useful information for faster translation of a novel drug from a preclinical experiment to a clinical protocol. This results in earlier proof-of concept and evaluation in man, thus accelerating the drug development time line. PET enables non-invasive organ-specific kinetic analysis in a living organism at tracer levels without interference of other biological parameters. It provides three-dimensional, functional nuclear imaging data from which

quantitative, temporal information about volume-regions of interest (vROI) can be derived. PET is attractive for both PK and tissue kinetics applications because of its exquisite quantitative sensitivity (below micromolar), non-invasiveness, specificity of anatomical delineation, and moderate resolution (1-2 mm in preclinical and 5-10 mm in clinical systems) for *in situ* measurements *in vivo*. Furthermore, the availability of natural radioisotopic labels (e.g., C-11 for natural carbon) and bioisosteric radionuclides (e.g., F-18 for H and OH) often supports synthesis of the required radioactive compound under investigation [20]. The vROI data from time-sequential (dynamic) images enables the investigator to derive quantitative time-dependent physiological parameters (rates) for regional drug concentrations and clearance parameters.

Small animal PET is suitable for many aspects of drug development using preclinical animal models, enabled especially by the development of dedicated small animal PET scanners over the past 25 years [21]. Large volumes of data are created during dynamic PET studies, and their storage, validation, processing and analysis are challenges not usually faced with data from *ex vivo* experiments.

PET kinetic analysis is not without challenges, which include scanner calibration, corrections for partial volume effects (signal contributions from nearby or overlapping non-target tissues), determination of the input function (an integral part of PET kinetic modeling), and reproducible, anatomically accurate volume delineation and vROI positioning for serial measurements. Low signal-to-noise ratios in vROI dynamic frames can compromise the statistical significance of kinetic parameter computation from time activity curves (TACs) [22,23]. Furthermore, because the PET signal detects radioactive atoms rather than drug molecules, care must be taken to resolve contributions of labeled metabolites, contaminants and degradation products to the observed count rates. The latter could be a major limitation of PET, but it can be overcome by additional analytical techniques to establish the presence of metabolites and the patency of the radiolabel. Of the many model- and data-driven methods of kinetic analysis using PET, anatomical PK compartmental analysis is most common. However, the input function, which represents the availability of the tracer at the tissue of interest, is necessarily required [24-26]. Interested reader are referred to Kuntner's comprehensive review of kinetic modeling of PET data [27].

Animal PET-based blood input function data are usually taken from heart ventricle vROIs. For [¹⁸F]FDG in mice, however, the heart ventricle cannot be analyzed because as a working muscle it actively imports and metabolically traps glucose (i.e., [¹⁸F]FDG), thereby steadily raising the amount of radioactivity trapped in the myocardium and thus resulting in false-positive blood measurements if the vROI includes muscle. Of several alternative sampling sites, successful analysis of vROIs placed over the vena cava have been reported [28,29]. The goal of the present study was to compare the basic PK parameters derived from classical blood-sampling data versus PET data derived from the *inferior vena cava*, following single bolus injections of either [¹⁸F]FAZA or [¹⁸F]FDG into the tail vein of mice bearing a mammary cancer. A second objective was to utilize PET image data to derive kinetic parameters for these radiopharmaceuticals in a murine tumor model, thereby demonstrating the additional power of the PET method in drug development.

METHODS and MATERIALS

Materials

Heparinized micro-hematocrit tubes, microcentrifuge tubes (1.5 µL) and reverse-phase micro TLC plates were purchased from Fisher Scientific (Burlington, ON, Canada). HPLC grade methanol and ethyl acetate originated from Caledon Laboratories Ltd. (Georgetown, ON, Canada) and sterile normal saline was obtained from Baxter Corporation (Toronto, ON, Canada). All other chemicals and reagents were obtained from Sigma-Aldrich (Oakville, ON, Canada) unless otherwise stated.

Radiometric analyses of blood samples

Radioactivity in blood samples and extracts was determined as counts per minute [CPM] using a WIZARD2 automatic gamma counter (Perkin Elmer, Waltham, MA, U.S.A.) and converted to Becquerels [Bq]. Radio-microTLC (microTLC) was performed on silica gel-coated glass plates (2.5cm x 7.5cm) using ethyl acetate as eluent. After development, plates were scanned for 2 min on an AR-2000 Bioscan scanner (Bioscan, Inc. USA; linearity 4-5 decades, sensitivity 100 DPM for ¹⁸F; counting efficiency 5%). Radioactive peaks were identified by co-chromatography with known reference standards

(e.g., FAZA; FDG). The radioactivity extraction efficiency for [^{18}F]FDG-containing blood using this technique was $91\pm 3\%$ ($n = 5$), and $91\pm 5\%$ ($n = 5$) for [^{18}F]FAZA containing blood. Distribution of radioactivity in plasma, cellular and protein fractions of whole blood samples was determined by separation and precipitation using methanol and gamma counting as described above.

Animals

Female BALB/c mice (20-22 g) (Charles River, Saint-Constant, QC, Canada), housed in the animal facility at the Cross Cancer Institute, were allowed free access to food and water under a 12-hour light/dark cycle. All animal experiments were carried out in accordance with guidelines of the Canadian Council on Animal Care (CCAC) and were approved by the local Cross Cancer Institute's Animal Care Committee.

Radiotracers

PET radiotracers used for this study were prepared at the Edmonton PET Center. [^{18}F]FAZA was synthesized by nucleophilic displacement of the corresponding 2',3'-di-acetyl-5'-tosyl azomycin arabinoside (15 mg) using Kryptofix/ K_2CO_3 /[^{18}F]fluoride complex [30]. Mild, base-catalyzed hydrolysis of the protecting acetyl substituents, followed by SepPak clean-up, afforded [^{18}F]FAZA in 20 % radiochemical yield. [^{18}F]FDG was synthesized by nucleophilic radiofluorination of mannose triflate with [^{18}F]fluoride in the presence of Kryptofix/ K_2CO_3 [31] using a TracerLab MX FDG Coincidence synthesizer.

PET Imaging

For PET experiments, murine EMT6 cells (10^6 cells in 100 μL of PBS) were injected into six female BALB/c mice. The EMT6 tumor-bearing mice were imaged 7–11 days post-injection with tumor sizes between ~ 300 and 400 mm^3 . The mice were fasted for 3-4 hours before imaging experiments. EMT6 tumor-bearing BALB/c mice were anesthetized with isoflurane in 40% oxygen/60% nitrogen (1 L/min), and body temperature was kept constant at 37°C for the entire experiment. Mice were immobilized in the prone position and positioned prone into the center of the field of view of a microPET[®] R4 scanner (Siemens Preclinical Solutions, Knoxville, TN, U.S.A.). A transmission scan for attenuation correction was not acquired. The amount of radioactivity [Bq] present in the injection solution in

a 0.5 mL syringe was measured with a dose calibrator (Atomlab 300; Biodex Medical Systems, Suffolk, NY). After the emission scan was started, radioactivity was injected after a delay of approximately 15 s. ^{18}F -labeled radiotracers (5 to 10 MBq in 100 to 150 μL of saline) were then injected through a tail-vein catheter. Data acquisition in 3D list mode continued for 60 min for [^{18}F]FDG and 90 min for [^{18}F]FAZA. List mode data were sorted into sinograms with 53 or 56 time frames (10x2, 8x5, 6x10, 6x20, 8x60, 10x120, 4 or 7x300 s). Time frames were reconstructed using the Ordered Subset Expectation Maximization (OSEM) or maximum a posteriori (MAP) reconstruction modes. No correction for partial-volume effects was performed. The image files were further processed using the ROVER v2.0.51 software (ABX GmbH, Radeberg, Germany). Masks encompassing 3D volume regions of interest (vROI) were set, and the vROIs were defined by thresholding. Voxels in each ROI contained PET data in units of Bq/mL or mean standardized uptake values [$\text{SUV}_{\text{mean}} = (\text{mean activity in vROI [Bq]} / \text{volume of vROI [mL]}) / (\text{injected activity [Bq]} / \text{body weight [g]})$, g/mL]. Time-activity curves (TAC) were generated from the dynamic scans. All semi-quantified PET data are presented as means \pm S.E.M. Time-activity curves were constructed using GraphPad Prism 5.0 (GraphPad Software).

Blood sampling

For blood collection experiments, normal female BALB/c mice (five), were given a bolus dose (20-30 MBq in 100 μL saline) of either [^{18}F]FDG or [^{18}F]FAZA *via* the jugular vein while under isoflurane anesthesia. Blood samples were collected by tail artery puncture at 5, 15, 30, 45 and 75 min post injection). To minimize trauma to the tail artery, a single sampling puncture was used for the first sample; following samples were taken by carefully removing the scab and collecting the sample (15 μL) from the bleed site into a calibrated heparinized micro-hematocrit capillary tube. The blood samples were radioassayed in a gamma well counter to determine radioactivity in the 'whole blood', then transferred into microcentrifuge tubes (1.5 mL) and frozen in dry ice to disrupt the blood cells. For work-up, the samples were thawed, transferred into microcentrifuge tubes (1.5 mL), vortex-mixed with methanol (30 μL), and then centrifuged (5 min; 11k rpm, MIKR 020 microfuge, Hettich Zentrifagen, Germany). The supernatant was transferred to new

polypropylene centrifuge tubes, and aliquots (2 μ L) of the supernatant were taken for chromatographic analysis.

Pharmacokinetic analysis

Non-compartmental PK analysis was applied to the concentration versus time-course data. The terminal elimination rate constant (λ_z) was estimated by determination of the negative slope (-slope) of the log-transformed blood concentration vs. time data. The terminal elimination half-life was calculated as $\ln(2)/\lambda_z$. The area under the curve ($AUC_{0-\infty}$) was calculated using the linear trapezoidal rule to sum all data from the time of dosing to the last measured concentration, plus the quotient of the last measured concentration divided by λ_z . Clearance (CL) was determined as the quotient of dose divided by $AUC_{0-\infty}$, and volume of distribution ($V_{d\text{area}}$) was determined by division of CL by λ_z .

Tumor kinetic modeling from dynamic PET imaging data

A reversible two-compartmental catenary model [32] with blood volume parameter has previously been used to specifically describe the tissue uptake of [^{18}F]FDG [33]. The same approach was also applied by Verwer et al. [34] for [^{18}F]FAZA (**Figure 2**).

To obtain the tumor kinetic parameters, besides the vROI over the tumor, a vROI defining the blood input was generated. The latter was obtained by thresholding the average *vena cava* content in early time frames which visualized the blood flow through the inferior vena cava briefly, for about 10 to 20 seconds post-injection. The plasma input TAC generated from this vROI was convolved with the compartmental model and numerically fitted to the tumor TACs of the same animal. This procedure was implemented in Matlab software (version R2016a), utilizing a Nelder-Mead simplex direct search. The fit was governed by minimization of the sum over all time points of square differences between the measured values and the model prediction. **Figure 3** shows a representative measured TAC as well as the curve obtained when the two-compartmental model was fitted to the data (dashed line). For illustration purposes only, an exploratory fit of a one-compartment model (dotted line) is also presented. It is noted that the latter achieves a much poorer agreement with the data, verifying that the measured data is indeed represented by a two-compartment

model, in accordance with the thorough analysis by Verwer et al. [34].

RESULTS

The presence of radioactive metabolites in the blood of [^{18}F]FDG- and [^{18}F]FAZA-dosed animals was examined by radio-microTLC. Up to 30 min post injection, the traces showed only single major radioactive peaks in whole blood extract following injection of either [^{18}F]FDG or [^{18}F]FAZA into mice (**Figure 4**).

To analyze blood compartment distribution, blood samples containing [^{18}F]FAZA and [^{18}F]FDG were separated into blood cells, protein and plasma fractions. Throughout 60 min post injection, [^{18}F]FAZA radioactivity was almost equally distributed between blood cells and plasma, with only a small fraction (~5%) associated with the protein fraction (**Figure 5A**). Chromatographic analysis of the plasma fraction showed that [^{18}F]FAZA was the major detectable component, accounting for over 95 % of plasma radioactivity at each time point. This is in agreement with literature reports that there is very little metabolism of [^{18}F]FAZA (<10 % at 70 min post injection) and that plasma-to-blood ratios remain close to unity [34].

PET images generated from a dynamic PET experiment 90 min ([^{18}F]FAZA) and 60 min ([^{18}F]FDG) post injection (**Figure 6**) confirm that [^{18}F]FDG is detected in the heart muscle over time, indicative of direct uptake and metabolic retention, while [^{18}F]FAZA is not accumulated by the healthy myocardium. For direct comparison of image-derived data for both radiotracers the inferior vena cava therefore represents a more suitable vROI.

Early PET images for [^{18}F]FDG and [^{18}F]FAZA during the perfusion phase at 7s, as well as 10 s, 1 min and 5 min post injection (**Figure 7**) show that both radiotracers pass through the inferior vena cava to the heart after tail vein injection, making it a suitable vROI sampling site for determining blood input function in mice. At 1 min p.i., differences in elimination pathways for both radiotracers become visible: [^{18}F]FDG is mainly cleared through the renal system while [^{18}F]FAZA shows more hepatobiliary clearance.

Image-derived time-activity curves (TACs) from vROIs over the heart and inferior vena cava are compared to classical blood sampling data from mice in **Figure 8**.

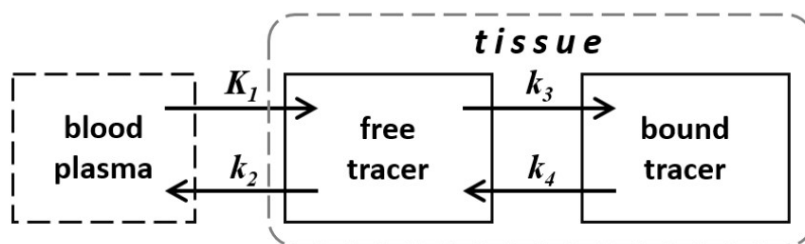


Figure 2. The two-compartment kinetic catenary model employed for both $[^{18}\text{F}]\text{FDG}$ and $[^{18}\text{F}]\text{FAZA}$; the first compartment represents free tracer inside a cell (cell membrane transport described by K_1 and k_2); the second compartment represents modified tracer molecules (phosphorylation in the case of $[^{18}\text{F}]\text{FDG}$ and reduction in the case of $[^{18}\text{F}]\text{FAZA}$); these processes and their reverse are described by the rate constants k_3 and k_4 , respectively. This ‘reversible’ configuration of the standard two compartment model is applied in PET image analysis to describe transport of unmetabolized tracer from blood into the tissue compartment and reversible binding or metabolism of the tracer in a separate compartment [32].

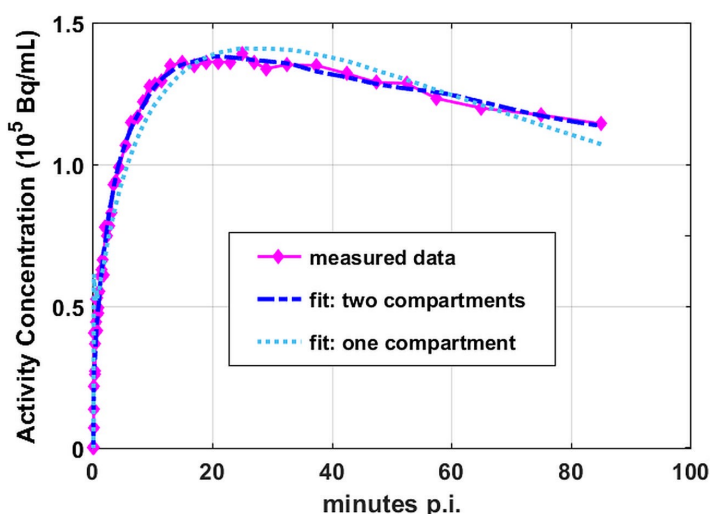


Figure 3. Measured data points for $[^{18}\text{F}]\text{FAZA}$ fitted with a two-compartment model (dashed) and one-compartment model (dotted); the two-compartment model provides an excellent reproduction of the measured data, in accordance with Verwer et al. [34].

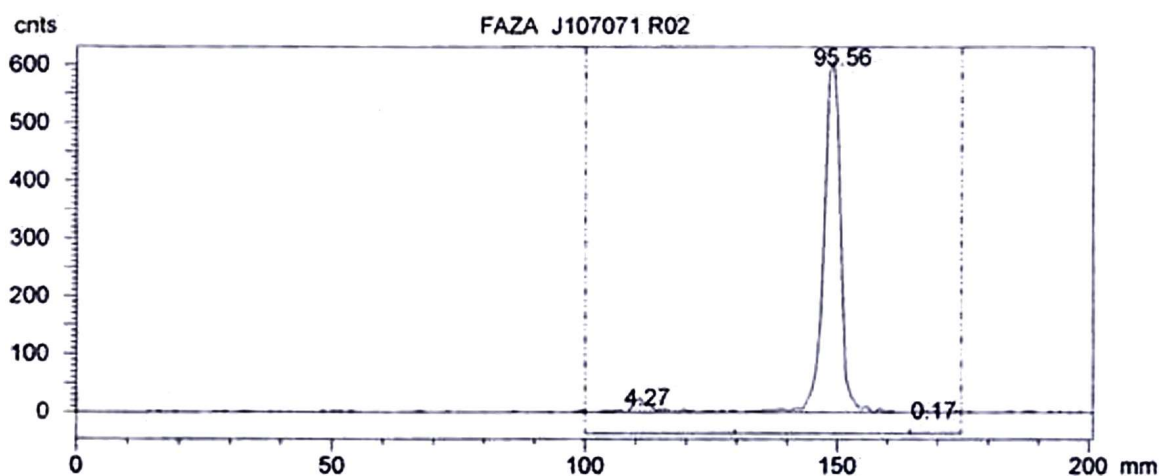


Figure 4. A representative radio-microTLC elution profile of the methanolic extract of arterial tail vein whole blood taken from a mouse at 15 min post injection following a single bolus dose of $[^{18}\text{F}]\text{FAZA}$ via jugular vein injection. The peak at 150 mm co-chromatographed with authentic FAZA and accounted for 96 % of the radioactivity on the plate; another region, accounting for 4 % of the extracted radioactivity was not identified. Similar profiles (not shown) were obtained after injection of $[^{18}\text{F}]\text{FDG}$.

For [¹⁸F]FDG, the vROI over the heart does not result in a clearance curve, whereas the vROI over the inferior vena cava does provide a blood clearance curve. For [¹⁸F]FAZA, both vROIs lead to clearance curves. Consequently, for comparison of these radiotracers in the same animal model, analysis of

the vROI over the inferior vena cava was chosen for calculation of kinetic parameters.

PK parameters for both radiotracers were also calculated from the blood samples and the PET image-derived data (**Table 1**).

Table 1. Pharmacokinetic parameters for [¹⁸F]FDG and [¹⁸F]FAZA.

Parameter	Blood samples (n=5)	PET inferior vena cava (n=3)	Blood / PETratio
[¹⁸F]FDG			
t _{1/2,λz} (min)	14.5 ± 2.2	12.1 ± 2.4	1.2 ± 0.3
CL (mL/min)	1.2 ± 0.3	0.9 ± 0.2	1.3 ± 0.4
Vd _{area} (mL)	24.0 ± 3.6	14.9 ± 3.7	1.6 ± 0.5
[¹⁸F]FAZA			
t _{1/2,λz} (min)	35.0 ± 7.3	29.1 ± 16.6	1.2 ± 0.7
CL (mL/min)	0.7 ± 0.2	0.5 ± 0.2	1.4 ± 0.7
Vd _{area} (mL)	35.1 ± 12.2	13.2 ± 2.1	2.7 ± 1.0

[¹⁸F]FDG and [¹⁸F]FAZA demonstrated similar values for t_{1/2,λz} in blood and overall blood CL, irrespective of whether the underlying data were based on blood samples or the image-derived input function. Values for Vd_{area} based on PET image-derived data, however, were somewhat lower than those derived from the blood-sampled data. This is the case for both [¹⁸F]FDG and [¹⁸F]FAZA, where the ratio (Blood/PET) is similar within statistical uncertainties, indicating a systematic underestimation of Vd_{area} with PET.

Distribution to target tissue, and final uptake and disposition of the radiotracer, can also be calculated from image-derived data. In the case of EMT6 tumor

analysis, a vROI can be placed over the tumor detected in the PET images (see **Figure 6** above). **Figure 9** depicts the TACs generated for tumor uptake for both [¹⁸F]FDG and [¹⁸F]FAZA. While EMT6 tumor uptake for [¹⁸F]FDG continuously increases over time, [¹⁸F]FAZA uptake is characterized by a maximum at around 20-30 min p.i., followed by a slight decrease / washout from tumor tissue. Together with the image-derived input function (in this case the data from the vROI over the inferior vena cava, **Figure 8**), kinetic parameters can be calculated from these data by fitting a two-compartment model to the experimental TACs.

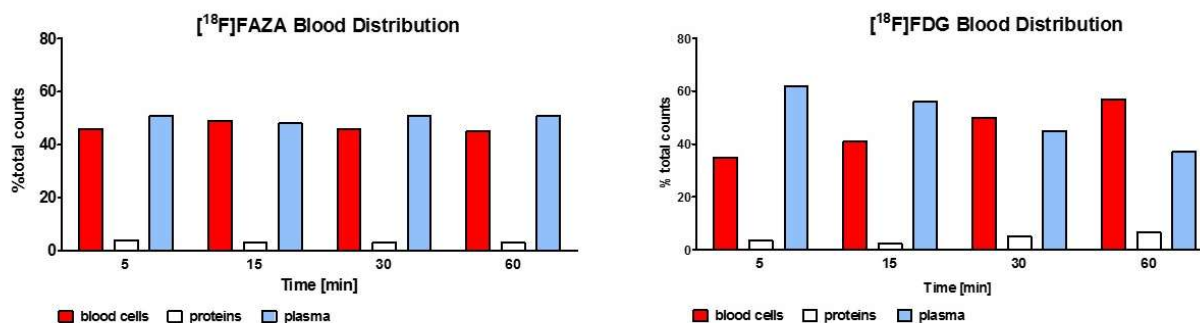


Figure 5. Distribution of radioactivity in blood fractions following injection of [¹⁸F]FAZA (Fig. 5A, left) and [¹⁸F]FDG (Fig. 5B, right) into BALB/c mice.

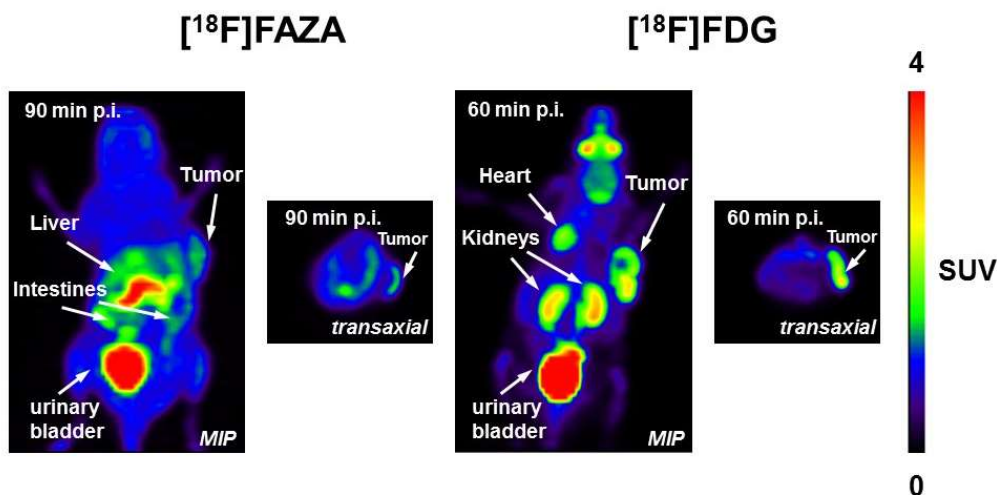


Figure 6. Maximum intensity projections (MIP) and transaxial PET images for $[^{18}\text{F}]\text{FAZA}$ (left at 90 min p.i.) and $[^{18}\text{F}]\text{FDG}$ (right at 60 min p.i.) in mammary EMT6 tumor bearing BALB/c mice. EMT6 tumors are visible with each radiotracer, the region of the heart only with $[^{18}\text{F}]\text{FDG}$.

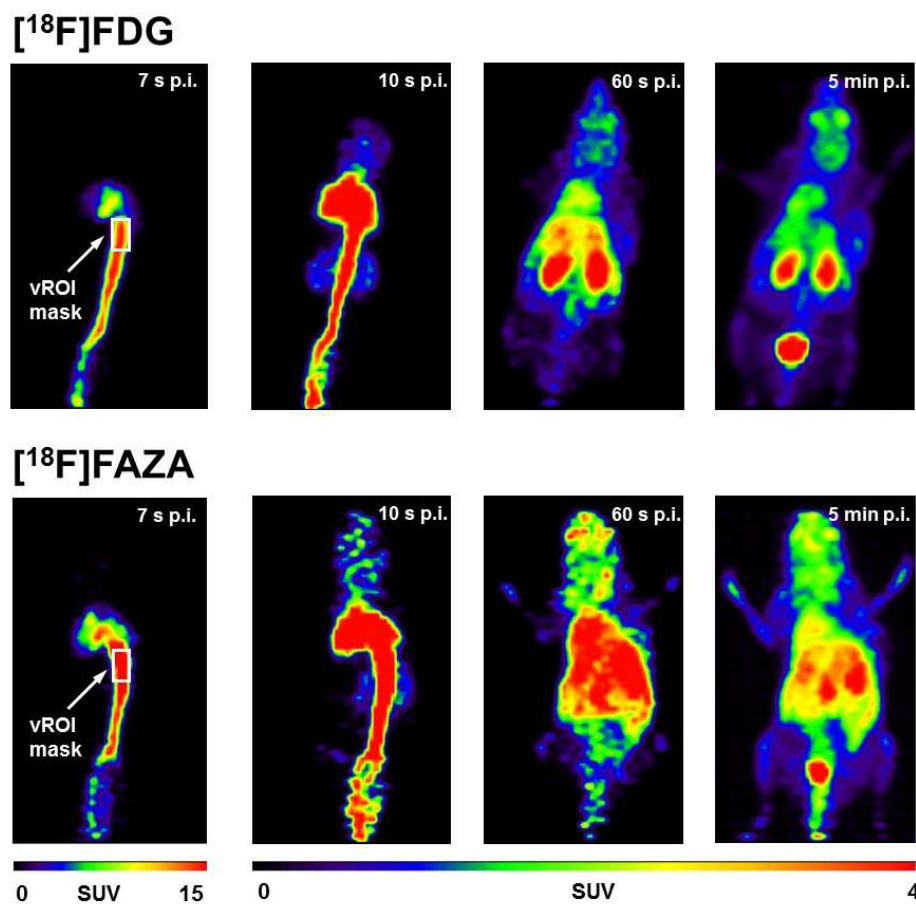


Figure 7. Maximum intensity projections (MIP) PET images for $[^{18}\text{F}]\text{FDG}$ (Top) and $[^{18}\text{F}]\text{FAZA}$ (Bottom) at 7, 10 and 60 s, and 5 min post injection into mammary EMT6 tumor bearing BALB/c mice. The arrows and boxes mark the vROI over the inferior vena cava chosen for the analysis of the image-derived input function.

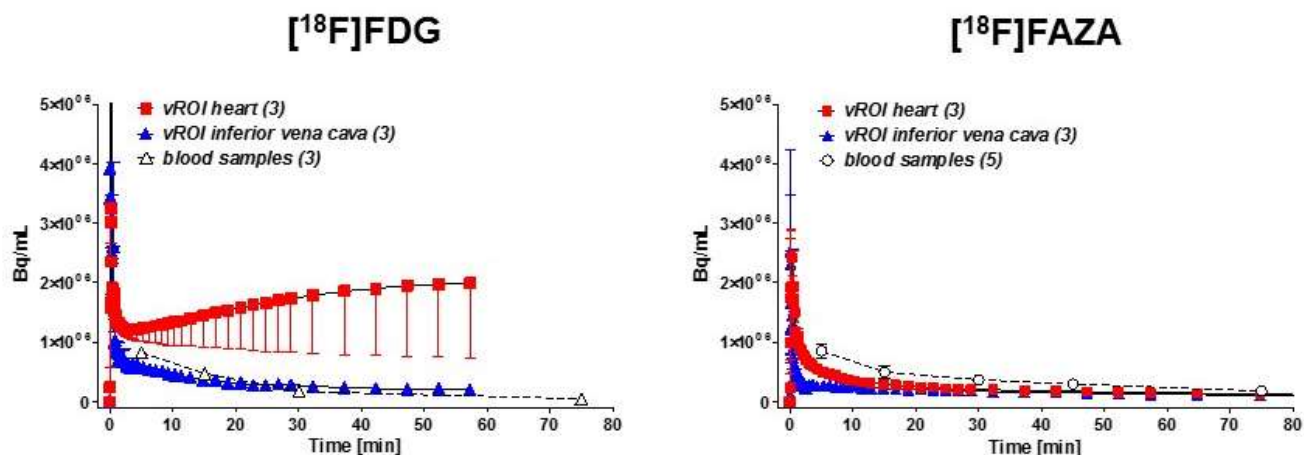


Figure 8. Time-activity curves (TACs) for vROI over the heart and inferior vena cava in comparison to data from direct blood samples after injection of [¹⁸F]FDG (left) and [¹⁸F]FAZA (right) into BALB/c mice. Data are shown as Bq per mL and mean ± SEM from 3 experiments.

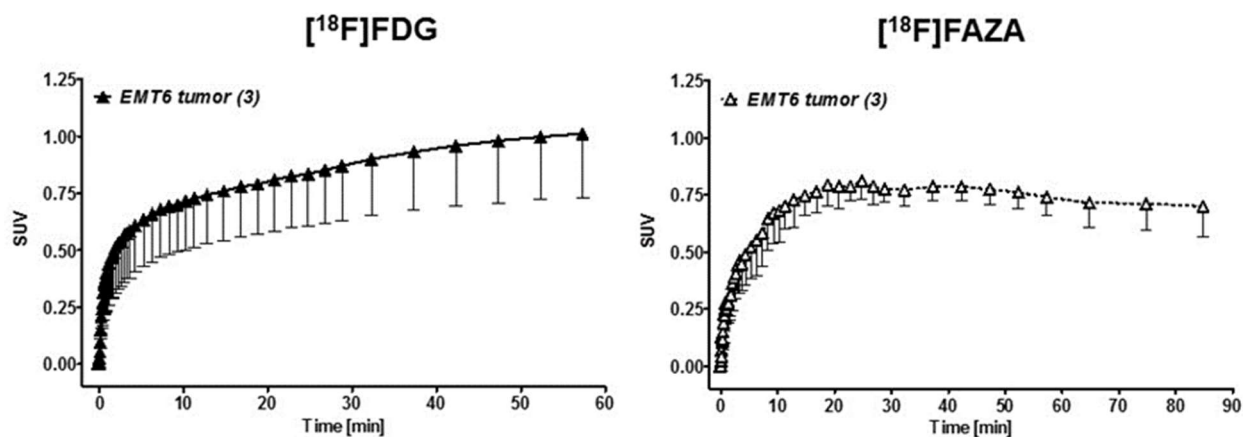


Figure 9. Time-activity curves (TACs) for vROI over EMT6 tumors after injection of [¹⁸F]FDG (left) and [¹⁸F]FAZA (right) into EMT6 tumor-bearing BALB/c mice. Data are shown as Standardized Uptake Values (SUV) and mean ± SEM from 3 experiments.

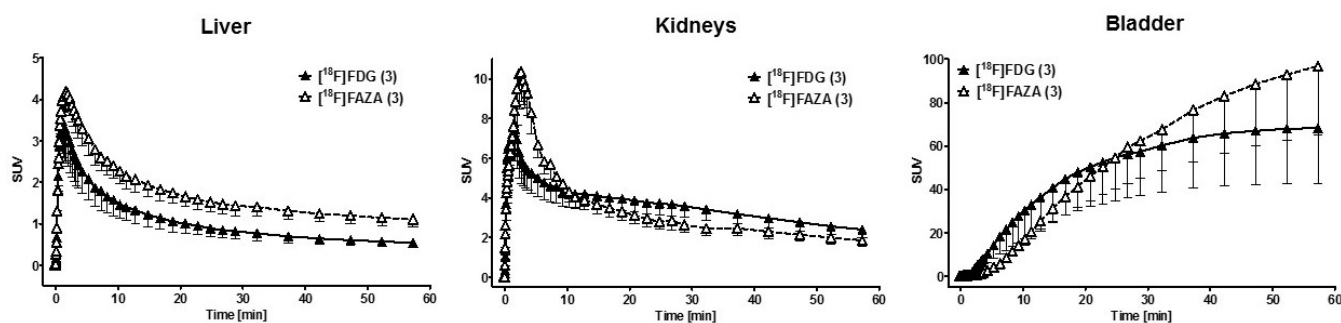
While use of the two-compartment model is well established for [¹⁸F]FDG [33], it was also suggested to be the best model for kinetic analysis of [¹⁸F]FAZA [34]. Based on these investigations, apparent kinetic parameters *for tumor* were calculated for both radiotracers in the EMT6 tumor model (Table 2).

In addition to tumor (target organ) uptake analysis, the TACs for liver, kidneys and bladder have also been generated for the same animals (Figure 10) in order to analyze clearance profiles. The TACs for these organs show clear differences in

the clearance patterns for each radiotracer. While the amount of radioactivity for hepatobiliary clearance is higher after injection of [¹⁸F]FAZA, [¹⁸F]FDG clearance is faster through the kidneys, leading to faster accumulation in the urinary bladder. Urinary excretion, presented as bladder radioactivity (Figure 10, right) shows that [¹⁸F]FDG excretion is essentially complete within 30-40 min, whereas [¹⁸F]FAZA radioactivity continues to be collected in the urinary bladder for the entire period (60 min) of observation and beyond.

Table 2. Apparent tumor kinetic parameters for [^{18}F]FDG and [^{18}F]FAZA in EMT6 tumor-bearing BALB/c mice; data (mean \pm SEM, n=3) were derived using a two compartment catenary model.

Parameter	[^{18}F]FDG	[^{18}F]FAZA
K_1 (mL/min/g)	0.139 ± 0.061	0.064 ± 0.009
k_2 (min^{-1})	0.231 ± 0.092	0.092 ± 0.029
k_3 (min^{-1})	0.059 ± 0.014	0.006 ± 0.003
k_4 (min^{-1})	0.007 ± 0.003	0.021 ± 0.016
$k_3/(k_2+k_3)$	0.257 ± 0.073	0.058 ± 0.031
$K_1 * [k_3/(k_2+k_3)]$ (mL/min/g)	0.027 ± 0.010	0.004 ± 0.002

**Figure 10.** Time-activity curves (TACs) for vROI over liver (left panel), kidneys (centre panel) and urinary bladder (right panel) after injection of [^{18}F]FDG and [^{18}F]FAZA into EMT6 tumor-bearing BALB/c mice. Data are shown as SUV and mean \pm SEM as a function of time after injection, from 3 experiments.

DISCUSSION

Animals in these imaging studies received tail vein injections through a properly placed tail vein catheter, whereas mice in the blood-sampling group received their radiotracer via jugular vein injection; both techniques were used in order to minimize the risk of undetected dose extravasation. It has been reported that up to 40% of improperly performed tail-vein injections can extravasate [35-37], a phenomenon that is readily monitored when imaging but is frequently undetected in other *in vivo* studies. In blood sampling protocols, cross contamination of blood taken from the tail is also a risk if the adjacent tissue contains radioactivity from an extravasated dose injected in that region. In the present experiments, there was no evidence of extravasation of dose in the imaging group, and blood samples were taken from the tail vein after injection of the doses into the jugular vein.

Radio-microTLC showed only single radioactive peaks corresponding to the respective injected radiotracer ([^{18}F]FDG or [^{18}F]FAZA), indicating that the amounts of radioactive metabolites in blood samples were negligible. This observation is critical to PK analysis using PET-derived data, because the PET data reflect total counts from all radioactivity present in the defined

vROI (i.e., not drug only, but also all radioactive metabolites). Cellular, but not circulating, metabolites of [^{18}F]FDG, including [^{18}F]FDG-6-P, [^{18}F]FDG-UDP, [^{18}F]FDG-1-P and 2-[^{18}F]FDG-1,6-di-P, have been reported, but there are no reports of the formation of circulating or urinary [^{18}F]fluoride [38-41]. No circulating metabolites of [^{18}F]FAZA have been reported. In the present study, in line with these literature reports, neither [^{18}F]FAZA or [^{18}F]FDG exhibited circulating metabolites by radio-microTLC and therefore blood- and image-derived data are directly comparable. Blood compartment analysis of [^{18}F]FDG revealed a shift of radioactivity from the plasma to the cellular fraction of whole blood with a concomitant decline in plasma radioactivity (Figure 5B). These observations are in line with literature reports that red cells and white cells both metabolically trap [^{18}F]FDG as [^{18}F]FDG-6-P, which accrues in all metabolically-active cells and cannot escape without (reverse) hydrolysis under the influence of hexokinase or glucose-6-phosphorylase. In human monocyte macrophages, for example, [^{18}F]FDG is trapped mainly as [^{18}F]FDG-6-P with lesser amounts of the diphosphate [^{18}F]FDG-1,6-P [42]. This metabolic process has been confirmed in [^{18}F]FDG labeling studies of both erythrocytes (which account for ~90 % of glucose metabolism by blood cells) [43] and

white blood cells (including lymphocytes, monocytes, neutrophils, eosinophils, and basophils) [44]. This irreversible nature of the dephosphorylation of FDG-6-P remains the basis for [^{18}F]FDG accumulation, and imaging, in all tissues [45]. For these reasons it has been suggested that the kinetics cellular radioactivity in blood be included in [^{18}F]FDG modeling [46].

The anatomical region of the heart can be utilized for measurement of the blood input function for [^{18}F]FAZA but not for [^{18}F]FDG, because the latter metabolically accrues over time in the myocardium, and current PET cameras do not have adequate spatial resolution to distinguish between blood and myocardium in the small, beating heart. The *inferior vena cava* was therefore chosen as vROI for measurement of the blood input function from PET data as shown in **Figure 6**, since it is the first region in which all of the radioactivity will be detected after injection into the tail vein of the mouse [28, 29].

Spillover from myocardial uptake (in the case of [^{18}F]FDG), partial volume effects and heart motion all contribute to the uncertainty of image-derived input functions from the region of the heart in small rodents [47, 48]. Corrections have been suggested based on direct blood sampling and determination of blood radioactivity, and successful application of factor analysis has been shown to resolve these issues [47]. The latter helps to overcome these limitations by deconvolving the blood and myocardial contributions to the cardiac time-activity curve [49]. Although myocardial uptake is not of concern for determination of the input function for [^{18}F]FAZA [34, 50], direct data comparison with [^{18}F]FDG can be achieved only by using the same methodology for both radiotracers to obtain input function data.

Direct comparison of the heart vs. inferior vena cava data shows that [^{18}F]FDG blood sampling values are more consistent with data from vROIs of the inferior vena cava, whereas the data from the vROI over the heart clearly show myocardial uptake of [^{18}F]FDG over time. In contrast, [^{18}F]FAZA blood sample data compare better with those derived from the vROIs over the heart. This illustrates that in either case, assumptions have to be made and the potential limitations for each method have to be taken into account when comparing data from two different radiotracers in the same mouse model. However, a recent study using [^{18}F]FDG in rats and mice has indeed established that the TAC derived

from a vROI over the vena cava is a suitable alternative for measurement of the image-derived input function without complications of repetitive blood sampling [28]. Using vROIs over the carotid arteries, ascending aorta or the heart, with corrections, have proven to be adequate for dynamic [^{18}F]FDG image analysis in humans, but for rodents, analysis of the inferior vena cava may represent the best alternative for [^{18}F]FDG image analysis.

Differences in $V_{d_{\text{area}}}$ between blood- and PET-derived data could be indicative of limitations owing to partial volume effect when analyzing vROIs over the inferior vena cava, but no attempts were made to apply partial volume corrections in the current study. On the other hand, analysis of blood half-life and blood clearance shows that these two values can be readily obtained from fast, straight-forward PET-image data analysis, allowing rapid, minimally invasive PK data to be derived from a first *in vivo* study using a radiolabeled compound. These results suggest that PET imaging is indeed an effective tool for providing useful PK data that can serve as basis for a faster translational drug development time-line, specifically accelerating the important step from preclinical *in vivo* to a clinical human study.

The precise extent and specific sites of metabolism for the two tested compounds are not known. Intravenous injection assures rapid, virtually ubiquitous distribution of these highly diffusible tracers during the early perfusion phase, followed quickly by redistribution, excretion and metabolism, phases that are recognizable by inspection of early PET images (**Figure 7**). Two organs, liver and kidney, quickly become involved in [^{18}F]FDG metabolism and excretion. While both radiotracers are cleared through the renal and the hepatobiliary systems, the roles of liver and kidney in [^{18}F]FAZA metabolism remain less well defined. Compared to [^{18}F]FAZA, renal clearance of [^{18}F]FD seems to be faster at the beginning, whereas clearance by liver is higher for [^{18}F]FAZA, resulting in even higher radioactivity levels in liver 60 min post injection.

[^{18}F]FDG is a difficult tracer to model because of several glucose-modulating physiological factors, including nutrition, hydration, physical stimulation and insulin. The liver normally removes two-thirds of the glucose from the blood, and the absorbed glucose is converted into glucose 6-phosphate by hexokinase and the liver-specific glucokinase. The kinetics of hepatic absorption of glucose and its radiotracer derivative [^{18}F]FDG are complicated by the dual blood supply from the hepatic artery (~90%)

and portal vein (~10%), which make accurate determination of the kinetic input function difficult [51]. Hepatic kinetic analysis based on the arterial input function (IF), the approach is used by most investigators, generates a systematic underestimation of tracer distribution in the liver [52]. In the current study, where the radiotracers are administered intravenously, there is no first pass effect; most of the drug available to the liver is arterial and therefore it is appropriate to base the kinetics on the arterial input function. Considering that hepatic blood flow in a ~20 g mouse is expected to be approximately 1.8 mL/min [53], and assuming liver is the major site of metabolism of these agents, the hepatic extraction ratios of [¹⁸F]FDG and [¹⁸F]FAZA are estimated to be 0.66 and 0.39, respectively.

Renal processing of [¹⁸F]FDG is qualitatively similar to glucose handling, with efficient glomerular filtration (FDG clearance rate 0.348/mL/min/100 g) from blood followed by tubular reabsorption (56% of FDG is reabsorbed) [54]. Tubular reabsorption of [¹⁸F]FDG is less efficient than for glucose, and it is effected via sodium-dependent glucose transporters (SGLTs), whereas high reabsorption of glucose is mediated by both SGLT and facilitative glucose transporters (GLUTs). The lower reabsorption of [¹⁸F]FDG than glucose is attributed to its lower affinity for both SGLTs and GLUTs [54, 55]. As a result, the CL of both of these agents could change in response to alterations in hepatic blood flow or intrinsic CL, with [¹⁸F]FDG being more sensitive to changes in hepatic blood flow than [¹⁸F]FAZA. It is of note that the ratios of [¹⁸F]FDG CL derived from PET to that derived from blood samples were 1.3 compared to 1.4 for [¹⁸F]FAZA. Given the expected higher hepatic extraction ratio of [¹⁸F]FDG compared to [¹⁸F]FAZA, this could explain why there was a higher CL for [¹⁸F]FDG. It is unlikely that [¹⁸F]metabolite(s) contribute to the observed differences in CL because no circulating metabolites of [¹⁸F]FDG or [¹⁸F]FAZA are reported. The calculated $V_{d_{area}}$ are indicative of significant distribution of the agents to the tissues, with distribution of [¹⁸F]FDG being higher than [¹⁸F]FAZA. V_d is innately limited by the fact that it carries no information about the physiological distribution of the agent; it is an intrinsic advantage of PET imaging that it provides this spatial information.

Because of the complex relationship between anesthesia and [¹⁸F]FDG kinetics, no attempt was made in the current studies to account for possible anesthesia effects. It is reported that cerebral glucose utilization of [¹⁸F]FDG in mice was reduced by both isoflurane (57%) and ketamine/xylazine (19%), and uptake by brain (%ID/g) was reduced by both ketamine/xylazine (54%) and isoflurane (37%); the complexity of these effects is borne out by their apparent ‘cross-over’ effects in the two measurements [56]. It is also reported that anesthetics like isoflurane and ketamine/xylazine impact both [¹⁸F]FAZA uptake in murine hypoxic tumor and at the same time alter oxygen tension in various tissues, suggesting that PK changes may be attributable to physiological effects [57]. In Sprague–Dawley rats, PK studies of [¹²³I]IAZA, a structurally-similar but more lipophilic analogue of [¹⁸F]FAZA, methoxyflurane anesthesia did not affect total radioactivity (i.e., [¹²³I]IAZA plus radioactive metabolites) kinetics, but the clearance of [¹²⁵I]IAZA was almost 3.5 times higher in the non-anesthetized animals than in the anesthetized group, pointing to metabolic influences as well as possible species differences in the effects of anesthetics on PK of this hypoxia imaging agent [57]. It is possible that the observed PK perturbations may lie in altered metabolism of the radioactive substrate, but it appears equally likely that the observed PK changes are attributable to the physiological effects of the anesthetic, including heart rate, respiratory rate, blood pressure and tissue perfusion. Although temperature effects on heart rate are reported to be minimal, significantly faster [¹⁸F]FDG uptake and washout kinetics are reported under controlled optimal heating [58]; animals were therefore maintained at 37 °C throughout the imaging period.

It is reported that warming and fasting also significantly reduce [¹⁸F]FDG uptake by brown adipose tissue and skeletal muscle in mice, and markedly improve visualization of tumor xenografts, with tumor uptake increased 4-fold and tumor-to-organ ratios increased up to 17-fold. Isoflurane anesthesia mildly increased blood glucose levels, whereas Ketamine/xylazine anesthesia caused marked hyperglycemia. Isoflurane increased the concentrations of radioactivity in liver, myocardium, and kidney. Thus, although the effects of anesthesia and animal protocols on radiotracer ([¹⁸F]FDG) kinetics have been the subject of numerous investigations, there are no predictive algorithms to compensate for them. Clearly, additional research

and standardization of all handling techniques in pre-clinical PET imaging is necessary to enhance the utility of micro-PET technique in pre-clinical drug development [57,59].

Calculated apparent kinetic data from PET experiments reveals that more [^{18}F]FDG is taken up by EMT6 tumor tissue than [^{18}F]FAZA (K_1), but also higher amounts of [^{18}F]FDG efflux from the tumor tissue, again compared to [^{18}F]FAZA (k_2). High amounts of [^{18}F]FDG are phosphorylated by hexokinase (k_3) and the de-phosphorylation rate is low (k_4). For [^{18}F]FAZA, the bioreduction rate is lower (k_3) than the single electron re-oxygenation rate (k_4). This leads to overall higher fraction of [^{18}F]FDG being retained (trapped by phosphorylation) by tumor tissue than [^{18}F]FAZA (trapped by bioreductive adduct formation): about a factor 4.4 separates the two tracers in this regard as evidenced by the branching ratio $k_3/(k_2+k_3)$. Taken together, this mammary mouse tumor model is characterized by high glucose metabolism ([^{18}F]FDG) versus a moderate hypoxic retention ([^{18}F]FAZA). The difference in overall amount of tracer progressing through the first to the second compartment and being retained there (the “trapping rate”) is even greater, as shown by the ratio of ~ 6.8 between [^{18}F]FDG and [^{18}F]FAZA for the quotient $K_1*[k_3/(k_2+k_3)]$.

CONCLUSION

This study provides a working example of the ability of functional dynamic PET imaging to reasonably determine PK parameters in small animals. In addition, dynamic PET allows for analysis of target organ uptake and retention in a specific model, e.g., in this study a mammary mouse tumor model. The comparative analysis in this study has demonstrated that it is feasible to use two different radiotracers, [^{18}F]FDG and [^{18}F]FAZA, in the same model to analyze tumor glucose metabolism and hypoxic fraction, respectively. This approach would translate well into the clinical setting and allow determination of both parameters in the same patient.

ACKNOWLEDGEMENT

The authors thank Dr. John Wilson, David Glendening and Blake Lazurko from the Edmonton PET Centre for ^{18}F production on a biomedical cyclotron. We further wish to thank Ali Akbari and Dr. William Sun for synthesis of [^{18}F]FAZA on an

automated synthesis unit and Jeff McPherson and Angela Westover for production of [^{18}F]FDG. This work was supported in part through CIHR POP 84164.

REFERENCES

- Challapalli A, Carroll L, Aboagye EO. Molecular mechanisms of hypoxia in cancer. *Clin Transl Imaging*, 2017; 5:225–253. DOI: 10.1007/s40336-017-0231-1.
- Wuest M, Wuest F. Positron emission tomography radiotracers for imaging hypoxia. *J Label Comp Radiopharm*, 2013; 56:244-250. DOI: 10.1002/jlcr.2997.
- Graham MM, Peterson LM, Link JM, Evans ML, Rasey JS, Koh WJ, Caldwell JH, Krohn KA. Fluorine-18-fluoromisonidazole radiation dosimetry in imaging studies. *J Nucl Med*, 1997; 38:1631-1636. PMID: 9739204.
- Kumar P, Stypinski D, Xia H, McEwan AJB, Machulla H-J, Wiebe LI. Fluoroazomycin arabinoside (FAZA): Synthesis, ^2H and ^3H -labelling and preliminary biological evaluation of a novel-2-nitroimidazole marker of tissue hypoxia. *J Label Comp Radiopharmaceuticals*, 1999; 42:3-16. DOI: 10.1002/(SICI)1099-1344(199901)42:1<3:AID-JLCR160>3.0.CO;2-H.
- Piert M, Machulla H-J, Picchio M, Reischl G, Ziegler S, Kumar P, Wester H-J, Beck R, McEwan AJB, Wiebe LI, Schwaiger M. Hypoxia-specific tumor imaging with [^{18}F]FAZA. *J Nucl Med*, 2005; 46:106-113. PMID: 15632040.
- Postema EJ, McEwan AJB, Riauka TA, Kumar P, Richmond D, Abrams DA, Wiebe LI. Initial results of hypoxia imaging using 1-alpha-D-(5-deoxy-5-[^{18}F]fluoroarabinofuranosyl)-2-nitroimidazole (^{18}F -FAZA). *Eur J Nucl Med Mol Imaging*, 2009; 36:1565-1573. DOI: 10.1007/s00259-009-1154-5. PMID: 19430784.
- Lopci E, Grassi I, Chiti A, Nanni C, Cicoria G, Toschi L, Fonti C, Lodi F, Mattioli S, Fanti S. PET radiopharmaceuticals for imaging of tumor hypoxia: a review of the evidence. *Am J Nucl Med Mol Imaging*, 2014; 4:365-384. PMID: 24982822.
- Savi A, Incerti E, Fallanca F, Bettinardi V, Rossetti F, Monterisi C, Compierchio A, Negri G Zannini P, Gianolli L, Picchio M. First evaluation of PET based human biodistribution and dosimetry of ^{18}F -FAZA, a tracer for imaging tumor hypoxia. *J Nucl Med*, 2017; 113:1224-1229. DOI: 10.2967/jnumed.113.122671.
- Pacák J, Tocik Z, Černý M. Synthesis of 2-deoxy-2-fluoro-D-glucose. *J Chem Soc D: Chem Commun*, 1969; 0:77–77. DOI: 10.1039/C29690000077.
- Ido T, Wan CN, Fowler JS, Wolf AP. Fluorination with molecular fluorine. A convenient synthesis of 2-

- deoxy-2-fluoro-D-glucose. *J Org Chem*, 1977; 42:2341-2342. DOI: 10.1021/jo00433a037.
11. Ido T, Wan C-N, Casella V, Fowler JS, Wolf AP, Reivich M, Kuhl D. Labeled 2-deoxy-D-glucose analogs. ¹⁸F-labeled 2-deoxy-2-fluoro-D-glucose, 2-deoxy-2-fluoro-D-mannose and ¹⁴C-2-deoxy-2-fluoro-D-glucose. *J Label Comp Radiopharm*, 1978; 14:175-183. DOI: 10.1002/jlcr.2580140204.
 12. Wiebe LI. FDG metabolism: *Quaecumque sunt vera...* *J Nucl Med*, 2001; 42:1679-1681. PMID: 11696639.
 13. Mitra E, Quon A. Positron emission tomography/computed tomography: the current technology and applications. *Radiol Clin North Am*, 2009; 47:147-160. DOI: 10.1016/j.rcl.2008.10.005.
 14. Nelson E. Kinetics of drug absorption, distribution, metabolism, and excretion. *J Pharm Sci*, 1961; 50:181-192. PMID: 13728276.
 15. Doogue MP, Polasek PM. The ABCD of clinical pharmacokinetics. *Ther Adv Drug Saf*, 2013; 4:5-7. DOI: 10.1177/204209861246335.
 16. Amitai N, Xin H, Kassel D, Kushon S. Advances in microsampling for in vivo pharmacokinetic studies. *The Column*, 2015; 11:2-7.
 17. Fan J, de Lannoy IA. Pharmacokinetics. *Biochem Pharmacol*, 2014; 87:93-120. DOI: 10.1016/j.bcp.2013.09.007.
 18. Welling PG, Balant LP. (Editors). *Handbook of Experimental Pharmacology*. Volume 110: Pharmacokinetics of Drugs, Springer-Verlag Berlin Heidelberg, 1994. DOI: 10.1007/978-3-642-78680-8.
 19. Cherry SR, Gambhir SS. Use of positron emission tomography in animal research. *ILAR J*, 2001; 42:219-232. PMID: 11406721.
 20. Wiebe LI. PET radiopharmaceuticals for metabolic imaging in oncology. *International Congress Series*, 2004; 1264:53-76. DOI: org/10.1016/j.ics.2003.12.102.
 21. DiFilippo FP, Patel S, Asosingh K, Erzurum SC. Small-animal imaging using clinical positron emission tomography/computed tomography and super-resolution. *Mol Imaging*, 2012; 11:210-219. PMID:22554485.
 22. Bian Z, Huang J, Ma J, Lu L, Niu S, Zeng D, Feng Q, Chen W. Dynamic positron emission tomography image restoration via a kinetics-induced bilateral filter. *PLoS ONE*, 2014; 9:e89282. DOI: org/10.1371/journal.pone.0089282.
 23. Verwer EE, Bahce I, van Velden FHP, Yaqub M, Schuit RC, Windhorst AD, Raijmakers P, Hoekstra OS, Lammertsma AA, Smit EF, Boellaard R. Parametric methods for quantification of ¹⁸F-FAZA kinetics in non-small cell lung cancer patients. *J Nucl Med*, 2014; 55:1772-1777. DOI: 10.2967/jnumed.114.141846.
 24. Gunn RN, Gunn SR, Turkheimer FE, Aston JAD, Cunningham TJ. Positron emission tomography compartmental models: A basis pursuit strategy for kinetic modeling. *J Cereb Blood Flow Metab*, 2002; 22:1425-1439. DOI: 10.1097/01.wcb.0000045042.03034.42.
 25. Mintun MA, Raichle ME, Kilbourn MR, Wooten GF, Welch MJ. A quantitative model for the in vivo assessment of drug binding sites with positron emission tomography. *Ann Neurol*, 1984; 15:217-227. DOI: 10.1002/ana.410150302.
 26. Phelps ME, Huang SC, Hoffman EJ, Selin C, Sokoloff L, Kuhl DE. Tomographic measurement of local cerebral glucose metabolic rate in humans with (F-18)2-fluoro-2-deoxy-D-glucose: validation of method. *Ann Neurol*, 1979; 6:371-388. DOI: 10.1002/ana.410060502.
 27. Kuntner C. Kinetic modeling in pre-clinical positron emission tomography. *Z Med Phys*, 2014; 24:274-285. DOI: 10.1016/j.zemedi.2014.02.003.
 28. Lanz B, Poitry-Yamate C, Gruetter R. Image-derived input function from the vena cava for ¹⁸F-FDG PET studies in rats and mice. *J Nucl Med*, 2014; 55:1380-1388. DOI: 10.2967/jnumed.113.127381.
 29. Thorn SL, deKemp RA, Dumouchel T, Klein R, Renaud JM, Wells RG, Gollob MH, Beanlands RS, DaSilva JN. Repeatable noninvasive measurement of mouse myocardial glucose uptake with ¹⁸F-FDG: Evaluation of tracer kinetics in a type 1 diabetes model. *J Nucl Med*, 2013; 54:1-8. DOI: 10.2967/jnumed.112.110114.
 30. Reischl G, Ehrlichmann W, Bieg C, Kumar P, Wiebe LI, Machulla H-J. Preparation of the hypoxia imaging PET tracer [¹⁸F]FAZA: Reaction parameters and automation. *Appl Radiat Isotopes*, 2005; 62:897-901. DOI: 10.1016/j.aparadiso.2004.12.004.
 31. Hamacher K, Coenen HH, Stocklin G. Efficient stereospecific synthesis of no-carrier-added 2-[¹⁸F]fluoro-2-deoxy-D-glucose using aminopolyether supported nucleophilic substitution. *J Nucl Med*, 1986; 27:235-238. PMID: 3712040.
 32. Van Den Hoff J. Principles of quantitative positron emission tomography. *Amino Acids*, 2005; 29:341-353. DOI: 10.1007/s00726-005-0215-8
 33. Phelps ME, Huang SC, Hoffman EJ, Selin C, Sokoloff L, Kuhl DE. Tomographic measurement of local cerebral glucose metabolic rate in humans with (F-18)2-fluoro-2-deoxy-D-glucose: validation of method. *Ann Neurol*. 1979; 6:371-88. DOI: 10.1002/ana.410060502
 34. Verwer EE, van Velden FHP, Bahce I, Yaqub M, Schuit RC, Windhorst AD, Raijmakers P, Lammertsma AA, Smit EF, Boellaard R. Pharmacokinetic analysis of [¹⁸F]FAZA in non-small cell lung cancer patients. *Eur J Nucl Med Mol Imaging*, 2013; 40:1523-1531. DOI: 10.1007/s00259-013-2462-3.
 35. Lee JJ, Chung JH, Kim SY. Effect of ¹⁸F-fluorodeoxyglucose extravasation on time taken for

- tumoral uptake to reach a plateau: animal and clinical PET analyses. *Ann Nucl Med*. 2016; 30: 525-533. doi: 10.1007/s12149-016-1090-y.
36. Vines DC, Green DE, Kudo G, Keller H. Evaluation of mouse tail-vein injections both qualitatively and quantitatively on small-animal pet tail scans. *J Nucl Med Technol* 2011; 39:1–7. DOI: 10.2967/jnmt.111.090951
37. Lasnon C, Dugué AE, Briand M, Dutoit S, Aide N. Quantifying and correcting for tail vein extravasation in small animal PET scans in cancer research: is there an impact on therapy assessment? *EJNMMI Research*, 2015; 5:61-68. DOI: 10.1186/s13550-015-0141-z.
38. Gallagher BM, Ansari A, Atkins H, Casella V, Christman DR, Fowler JS, Ido T, MacGregor RR, Som P, Wan CN, Wolf AP, Kuhl DE, Reivich M. Radiopharmaceuticals XXVII. ^{18}F -labeled 2-deoxy-2-fluoro-D-glucose as a radiopharmaceutical for measuring regional myocardial glucose metabolism in vivo: tissue distribution and imaging studies in animals. *J Nucl Med*, 1977; 18:990–996. PMID: 903484.
39. Suolinna EM, Haaparanta M, Paul R, Härkönen P, Solin O, Sipilä H. Metabolism of 2- ^{18}F fluoro-2-deoxyglucose in tumor bearing rats: chromatographic and enzymatic studies. *Int J Rad Appl Instrum B*, 1986; 13:577–581. DOI: 10.1016/0883-2897(86)90141-8.
40. Kanazawa Y, Umayahara K, Shimmura T, Yamashita T. ^{19}F NMR of 2-deoxy-2-fluoro-D-glucose for tumor diagnosis in mice. An NDP-bound hexose analog as a new NMR target for imaging. *NMR Biomed*, 1997; 10:35-41. PMID:9251114.
41. Kaarstad K, Bender D, Bentzen L, Munk OL, Keiding S. Metabolic fate of ^{18}F -FDG in mice bearing either SCCVII squamous cell carcinoma or C3H mammary carcinoma. *J Nucl Med*, 2002; 43:940-947. PMID: 12097467.
42. Deichen JT Prante O, Gack M, Schmiedehausen K, Kuwert T. Uptake of ^{18}F fluorodeoxyglucose in human monocyte-macrophages in vitro. *Eur J Nucl Med Mol Imaging* 2003; 30; 267-273. PMID: 12552345.
43. Matsusaka Y, Nakahara T, Takahashi K, Iwabuchi Y, Nishime C, Kajimura M, Jinzaki M. ^{18}F -FDG-labeled red blood cell PET for blood-pool imaging: preclinical evaluation in rats. *EJNMMI Res*. 2017; 7: 19-29. doi: 10.1186/s13550-017-0266-3; PMID: PMC5328895; PMID: 28244021
44. Pellegrino D, Bonab AA, Dragotakes SC, Pitman JT, Mariani G, Carter EA. Inflammation and Infection: Imaging Properties of ^{18}F -FDG–Labeled White Blood Cells Versus ^{18}F -FDG *J Nucl Med*, 2005; 46; 1522-1530. PMID: 16157536
45. Wang G, Qi J. Direct estimation of kinetic parametric images for dynamic PET. *Theranostics*. 2013;3(10):802–15.
46. AlfMF, Martić-Kehl MI, Schibli R, Krämer SD. FDG kinetic modeling in small rodent brain PET: optimization of data acquisition and analysis. *EJNMMI Res*. 2013; 3: 61. doi: 10.1186/2191-219X-3-61; PMID: PMC3737082; PMID: 23915734.
47. Kim J, Herrero P, Sharp T, Laforest R, Rowland DJ, Tai Y-C, Lewis JS, Welch MJ. Minimally invasive method of determining blood input function from PET images in rodents. *J Nucl Med*, 2006; 47:330-336. PMID:16455640.
48. Dandekar M, Tseng JR, Gambhir SS. Reproducibility of ^{18}F -FDG microPET Studies in Mouse Tumor Xenografts. *J Nucl Med*, 2007; 48:602-607. DOI: 10.2967/jnumed.106.036608.
49. Meyer PT, Circiumaru V, Cardi CA, Thomas DH, Bal H, Acton PD. Simplified quantification of small animal ^{18}F FDG PET studies using a standard arterial input function. *Eur J Nucl Med Mol Imaging*, 2006; 33:948-954. PMID:16699768.
50. Chapman DW, Jans HS, Ma I, Mercer JR, Wiebe LI, Wuest M, Moore RB. Detecting functional changes with ^{18}F FAZA in a renal cell carcinoma mouse model following sunitinib therapy. *EJNMMI Research*, 2014; 4:27-37. DOI: 10.1186/s13550-014-0027-5.
51. Munk OL, Bass L, Roelsgaard K, Bender D, Hansen S, Keiding S. Liver kinetics of glucose analogs measured in pigs by PET: importance of dual-input blood sampling. *J Nucl Med*. 2001;42(5):795–801)
52. Garbarino S, Vivaldi V, Delbary F, Caviglia G, Piana M, Marini C, Capitanio S, Calamia I, Buschiazzo A, Sambuceti G. A new compartmental method for the analysis of liver FDG kinetics in small animal models. *EJNMMI Research* 2015; 5: 35-44. doi.org/10.1186/s13550-015-0107-1
53. Davies B, Morris T. Physiological parameters in laboratory animals and humans. *Pharm Res*, 1993; 10:1093-1095. PMID:8378254.
54. Moran JK, Lee HB, Blaufox MD. Optimization of urinary FDG excretion during PET imaging. *J Nucl Med* 1999; 40; 1352-1357.
55. Kobayashi M, Shikano N, Nishii R, Kiyono Y, Araki H, Nishi K, Oh M, Okudaira H, Ogura M, Yoshimoto M, Okazawa H, Fujibayashi Y, Kawai K. Comparison of the transcellular transport of FDG and D-glucose by the kidney epithelial cell line, LLC-PK1. *Nucl Med Commun*. 2010; 31: 141-146. doi: 10.1097/MNM.0b013e328333bcf5.
56. Toyama HI, Ichise M, Liow JS, Modell KJ, Vines DC, Esaki T, Cook M, Seidel J, Sokoloff L, Green MV, Innis RB. Absolute quantification of regional cerebral glucose utilization in mice by ^{18}F -FDG small animal PET scanning and 2- ^{14}C -DG autoradiography. *J Nucl Med*. 2004; 45:1398-1 PMID: 15299067 405.

57. Mahling M, Fuchs K, Thaiss WM, Maier FC, Feger M, Bukala D, Harant M, Eichner M, Reutershan J, Lang F, Reischl G, Pichler BJ, Kneilling M. A Comparative pO₂ Probe and [¹⁸F]-Fluoro-Azomycinarabino-Furanoside ([¹⁸F]FAZA) PET Study Reveals Anesthesia-Induced Impairment of Oxygenation and Perfusion in Tumor and Muscle. PLoS ONE, 2015, 10: e0124665. doi.org/10.1371/journal.pone.0124665.
58. Goetz C, Podein M, Braun F, Weber WA, Choquet P, Constantinesco A, Mix M. Influence of Animal Heating on PET Imaging Quantification and Kinetics: Biodistribution of ¹⁸F-Tetrafluoroborate and ¹⁸F-FDG in Mice. J Nucl Med. 2017; 58: 1162-1166. doi: 10.2967/jnumed.116.177949.
59. Fueger BJ, Czernin J, Hildebrandt I, Tran C, Halpern BS, Stout D, Phelps ME, Weber WA. Impact of animal handling on the results of ¹⁸F-FDG PET studies in mice. J Nucl Med. 2006; 47: 999-1006. PMID: 16741310